Physics of Plasmas

First self-consistent simulations of trapped electron clouds in a gyrotron gun and comparison with experiments

Cite as: Phys. Plasmas **30**, 030702 (2023); https://doi.org/10.1063/5.0136340
Submitted: 25 November 2022 • Accepted: 10 February 2023 • Published Online: 01 March 2023

G. Le Bars, J. Loizu, J.-Ph. Hogge, et al.

Physics of Plasmas LETTER scitation.org/journal/php

First self-consistent simulations of trapped electron clouds in a gyrotron gun and comparison with experiments

Cite as: Phys. Plasmas **30**, 030702 (2023); doi: 10.1063/5.0136340
Submitted: 25 November 2022 · Accepted: 10 February 2023 ·
Published Online: 1 March 2023

G. Le Bars,[1,a)] J. Loizu,[1] J.-Ph. Hogge,[1] S. Alberti,[1] F. Romano,[1] J. Genoud,[1] and I. G. Pagonakis[2]

AFFILIATIONS

[1]Ecole Polytechnique Fédérale de Lausanne (EPFL), Swiss Plasma Center (SPC), CH-1015 Lausanne, Switzerland
[2]ETH Zürich, Zürich, Laboratory of Physical Chemistry, CH-8093 Zürich, Switzerland

[a)]Author to whom correspondence should be addressed: guillaume.lebars@epfl.ch

ABSTRACT

We report on the initial validation of the novel code FENNECS, which simulates the spontaneous formation of trapped electron clouds in coaxial geometries with strong externally applied azimuthal flows and in the presence of a residual neutral gas. For this purpose, a realistic gyrotron electron gun geometry is used in the code, and a self-consistent electron cloud build-up is simulated. The predicted electronic current resulting from these clouds that is collected on the gun electrodes is simulated and successfully compared with the previous experimental results for configurations with different externally applied electric and magnetic fields. These different configurations effectively modify the size and depth of the trapping potential wells responsible for the confinement of the electron clouds. This investigation also provides further insight into the link between potential well depth and resulting electronic current.

Gyrotrons are planned to play a key role in heating magnetically confined fusion plasmas through electron cyclotron resonance heating.[1–4] In addition, gyrotrons can be used to drive the electronic current in tokamaks and to stabilize some types of plasma instabilities that could cause disruptions of the fusion plasma.[1–3] These gyrotrons are high power microwave sources operating in the range of 0.1–2 MW and 50–300 GHz and are capable of operating in pulsed and CW modes. These devices rely on the excitation of the electron cyclotron resonance maser instability of a magnetized weakly relativistic electron beam flowing through a cylindrical cavity.[5,6] The development and design of gyrotrons are challenging on many levels, one of which is the possible trapping of secondary electrons (i.e., not belonging to the main electron beam) in the electron gun region of the gyrotron. These electrons can be trapped due to the presence of electrostatic potential wells created by the combination of electric and magnetic fields and are similar in nature to the ones used to trap non-neutral plasmas in Penning–Malmberg traps.[7] These wells are present for electrons when the electric potential has a local maximum along a magnetic field line, and their depth is defined as the potential difference between this local maximum and the highest closest local minimum on each side along the magnetic field line.[8,9] Once trapped, the electrons can ionize the residual neutral gas present in the vacuum vessel and promote the formation of high-density electron clouds. A steady leakage of the electron clouds, for example, due to collisional-driven cross field drifts, leads to the collection of potentially damaging currents on the gun electrode surfaces and sometimes even to an arcing event.[8–10] In addition, these resulting currents need to be sustained by a polarizing power supply (PS) that is generating the accelerating electric field for the main beam. Typically, exceeding a critical current as low as a few tens of mA will cause the PS to switch itself off and, therefore, prevent the gyrotron operation. Furthermore, the presence of these clouds could also perturb the accelerating electric field of the main electron beam, modifying the beam characteristics and reducing the efficiency of the beam–wave interaction in the cavity. To avoid such issues, the current solution is to prevent the formation of any potential well in the electron gun at the nominal magnetic field by carefully adapting the electrodes shape. This, however, introduces stringent constraints in the design of gyrotrons. A better understanding of the dynamics of these trapped electrons, and on the relation between the potential well and the currents collected on the electrodes, would be very beneficial to define relaxed design criteria for future electron guns. A numerical model has recently been derived to study

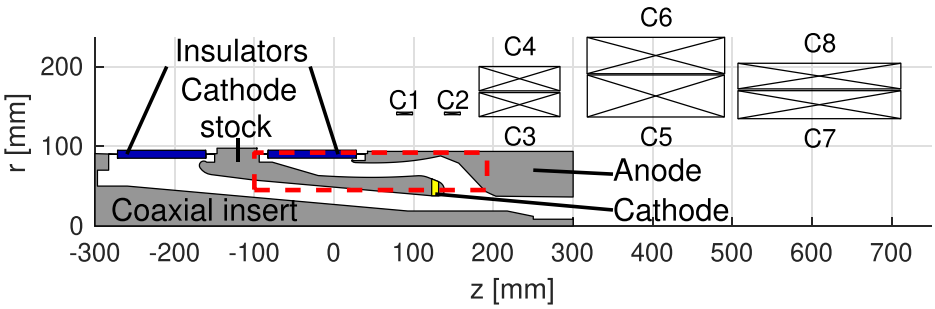

FIG. 1. Geometry of the refurbished electron gun and of the superconducting coils C1–C8 generating the magnetic field. An azimuthal symmetry is implied. The red dashed rectangle represents the limits of the simulation domain. Gray denotes a metallic material, and blue denotes an insulator. The yellow section represents the emissive ring where the main electron beam is produced.

the dynamics of trapped electron clouds, and scaling laws have been proposed to explain and quantify the collection of currents on the electrodes.[9] In this manuscript, we present the first validation of this model by comparing experimental results with numerical simulations using the actual geometry of a gyrotron electron gun. This is an important milestone that increases the confidence in the numerical model. It also shows the capability of this model to predict the risk of problematic currents in future gyrotron electron guns and that this model can facilitate the design phase of the gun geometry. We would like to remark that this work also represents the first validation of simulations of trapped electron clouds in gyrotron guns, ever performed against experiments.

The problem of trapped electron clouds has been observed in some gyrotrons such as in the magnetron injection gun (MIG) developed for the initial prototype of the 2 MW 170 GHz coaxial gyrotron planned for ITER.[11] In this gun, the nominal accelerating bias could not be sustained due to trapped secondary electrons, which lead to excessive currents flowing through the PS. The presence of a potential well caused excessive currents in the CW operation (without electron beam), and the gun also suffered from adiabatic trapped electrons,[8] which did not allow the operation of the gyrotron at the nominal parameters even in short pulses. These effects hindered the nominal operation of the gyrotron and limited the efficiency and power output.[12,13] A new geometry was then designed in which a special attention was paid to avoid the formation of any potential well, for the nominal magnetic field of the gyrotron.[14] This particular refurbished gun geometry is presented in Fig. 1. The added benefit of this refurbished geometry for studying electron trapping is the capability to create potential wells of different shapes and depths by slightly varying the magnetic field lines topology, from the nominal one, in the gun region. This can be achieved by varying the current I_{cc} flowing through two particular control coils (C3 and C4 in Fig. 1). It was experimentally shown that for some magnetic field topologies where a potential well is present, the voltage stand-off capabilities of the accelerating electrodes were significantly worsened.[14] This means that the maximum bias $\Delta\phi$, which could be applied to the electrodes without measuring any current flowing between them, was significantly reduced. For this experiment, a dummy gyrotron gun was built according to the design of the refurbished prototype of the 2 MW 170 GHz coaxial gyrotron planned for ITER. In the dummy-gun, no emissive ring was installed; therefore, no electron beam could be produced. The goal of the dummy-gun was to test the voltage stand-off capabilities of the design without the magnetic field and at the nominal magnetic field configuration for operating the gyrotron at the nominal power. During the experimental campaign, the voltage stand-off was also tested with increasing potential well depths U_{well} and size by decreasing the control coil currents as shown in Figs. 2 and 3. For a set of control coil currents, the maximum bias $\Delta\phi$, which could be applied without observing problematic currents (without tripping the PS), was measured up to the PS limits of 105 kV.[14] The results of these experiments are shown in Fig. 6 (red dots and white dashed line) and show a sharp reduction in the voltage stand-off below a control coil current of $I_{cc} = 5.3$ A. Figure 6 also shows the lines of constant potential well depth U_{well} (red dashed line). It is important to note that, for some configurations, a potential well could be present while no problematic currents were measured, which is a good indication that relaxed MIG design criteria could be defined.

In conjunction to these experimental studies, a numerical study of these electron clouds dynamics has been performed and is the subject of this Letter. We used a 2D (r, z) axisymmetric electrostatic particle-in-cell (PIC) code called FENNECS (Finite Element Non-Neutral Electron Clouds Simulator) developed at the Swiss Plasma Center (SPC).[9] This code solves the Vlasov–Poisson equations for the distribution function of electrons with the inclusion of a collision

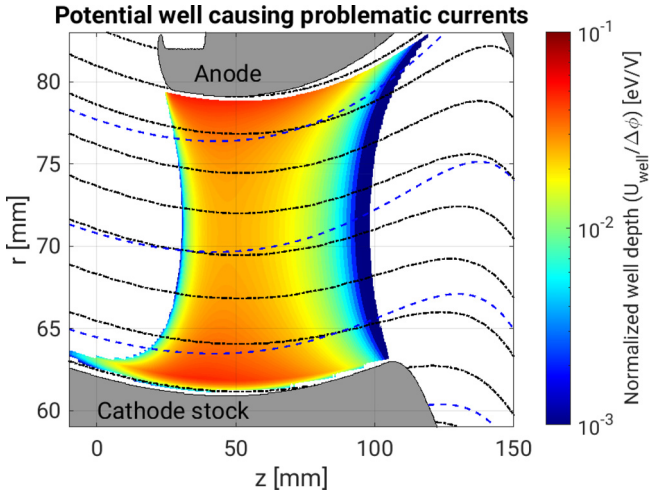

FIG. 2. Detail of the trapping region and normalized vacuum potential well formed for a control coil current $I_{cc} = 4.6$A. In the white region, the well depth is 0 and the black dashed–dotted lines represent the magnetic field lines for $I_{cc} = 4.6$A. The blue dashed line represents the magnetic field lines for a magnetic configuration where $I_{cc} = 6.2$A and no potential well is present.

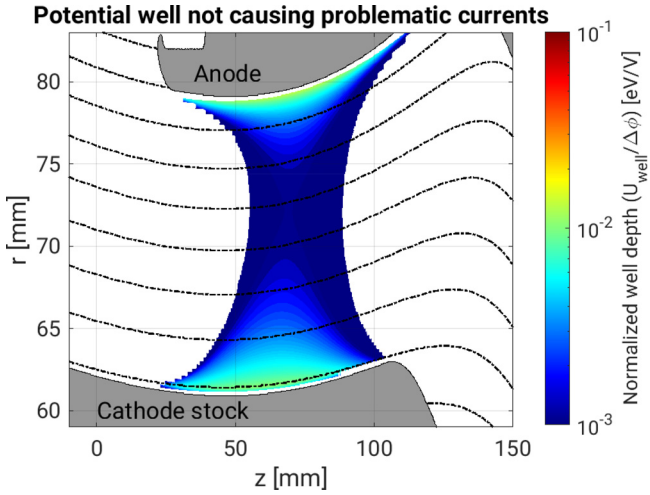

FIG. 3. Detail of the trapping region and normalized vacuum potential well formed for a control coil current $I_{cc} = 5.6$A. In the white region, the well depth is 0 and the dashed–dotted lines represent the magnetic field lines.

operator that describes electron–neutral elastic and inelastic (ionizing) collisions. By solving these equations, the code is capable of simulating the self-consistent evolution of the potential well and of the trapped electron cloud by taking into account the space-charge effects of the electrons and by simulating the ionization of the residual neutral gas (RNG) present in the vacuum vessel. The RNG is simulated as a background gas of uniform density at room temperature.[9] The ions released during the ionization processes are considered not magnetized due to their large Larmor radius and are accelerated toward the cathode and captured on the electrode surface after a time $\tau_{\text{loss}} \approx 10^{-8}$s much faster than the expected cloud formation time $\tau_f \approx 10^{-2} - 10$ s. For this reason, they are not simulated in the code. It is important to note that both in the experiment and in the simulations, the cathode was cold and the main electron beam of the gyrotron was, therefore, not generated. The primary electrons that ionize the RNG and start the cloud formation are expected to be generated either by field-emission[15] or by ionization of the RNG due to background radiation. This effect is simulated in the code by an *ad hoc* volumetric source covering the full simulation domain. The electron production rate of this source S is also adapted such that this source is negligible compared to the ionization rate S_i of the RNG by trapped electrons ($S \ll S_i$). The Poisson solver uses a finite element method based on weighted extended b-splines,[16] and the particle pusher uses the Boris algorithm.[17] To simulate the complex geometry of the electrodes, some modifications have been done to the FENNECS code. The geometric weight definition used to impose the Dirichlet boundary conditions in the Poisson solver has been adapted. Indeed, the metallic boundary conditions surfaces (Dirichlet) can now be defined using b-spline curves and the geometric weight is now based on a smoothed distance function to the metallic wall.[16] This change allows the simulation of arbitrary geometries, and, in particular, the simulation of the complex and realistic electron gun geometry in the code. Furthermore, the magnetic field applied by the eight superconducting coils, C1–C8 in Fig. 1, is precomputed numerically by solving the Biot–Savart equation and provided as an input to the code. It is then possible from the simulations to measure the effect of the potential shape and depth on the trapped electron cloud density and on the amplitude of the electronic current collected on the electrode surfaces. The simulations show the formation of a quasi-steady state, as a balance between the source of electrons caused by the ionization of the RNG, and a sink imposed by collisional driven cross field radial drifts causing the electrons to hit the electrodes and be captured. Due to the trapping geometry, the electron clouds form a ring radially confined inside coaxial electrodes as seen in Fig. 4 and are located in the regions where the self-consistent well including space-charge effects is the deepest as seen in Fig. 5. To compute the potential well depth U_{well}, the electric potential ϕ is evaluated along a set of magnetic field lines. For each field line and each position s_0 along the field line, the closest minimum of electric potential $\min(\phi(s))$ is determined on each side of the position considered. The highest of these minima is then subtracted from the local potential with $U_{well}(s_0) = \phi(s_0) - \max(\min(\phi(s)|s < s_0), \min(\phi(s)|s > s_0))$. The well depth is then transposed from field line coordinates to cylindrical coordinates. This implies that the vacuum potential well shape is purely defined by the magnetic field topology and the electrodes geometries. For a fixed I_{cc}, the vacuum well depth is, therefore, directly proportional to the applied bias $\Delta\phi$ and a normalized depth can be defined as $U_{well}(r,z)/\Delta\phi$ (Figs. 2 and 3).

A set of 136 simulations were carried out by scanning the control coil current in the range $I_{cc} = 4.6$–6.8A with 0.2A steps and biases in the range $\Delta\phi = 5 - 95$kV with 10kV steps covering the scanned parameters of the experimental results. The bias scan was even extended with biases $\Delta\phi = 115, 150,$ and 200 kV, shown by the hatched gray region of Fig. 6, which could not be achieved experimentally due to PS limitations. In each simulation, the time step is $\Delta t = 8 \times 10^{-12}$s $\approx 0.05/f_{ce}$, where $f_{ce} = eB/(2\pi m_e)$ is the cyclotron frequency; e is the electron charge; $B \approx 0.23$T is the magnetic field amplitude in the trapping region; and m_e is the electron rest mass. The Poisson equation was solved using a finite element method based on

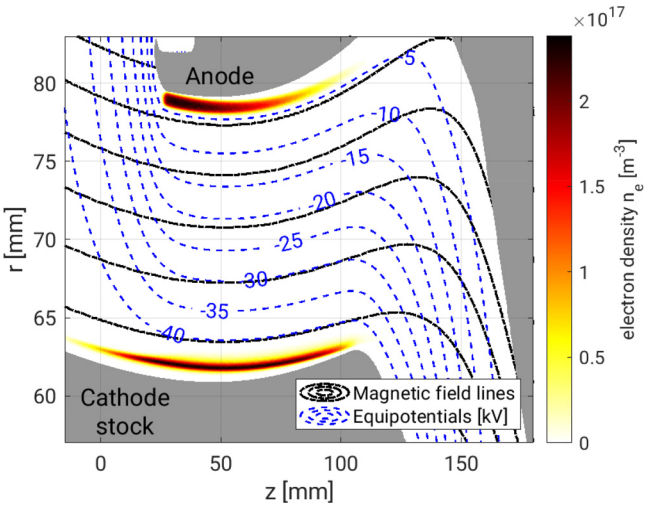

FIG. 4. Detail of the trapping region and steady-state electron density for a control coil current $I_{cc} = 4.6$A and an applied PS bias $\Delta\phi = 45$ kV. The black dashed–dotted lines represent the magnetic field lines, and the blue dashed lines represent the electric equipotential lines.

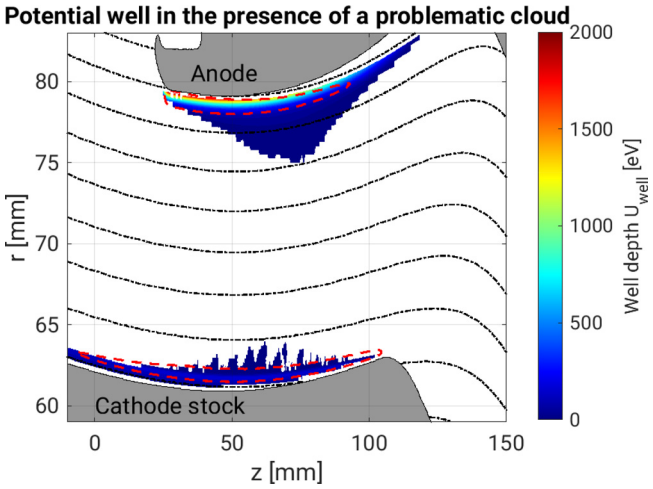

FIG. 5. Detail of the trapping region and self-consistent potential well for a control coil current $I_{cc} = 4.6$ A and an applied PS bias $\Delta\phi = 45$ kV. The black dashed–dotted lines represent the magnetic field lines, and the red dashed line indicates the outline of the cloud where $n_e = 0.1\,\max(n_e)$.

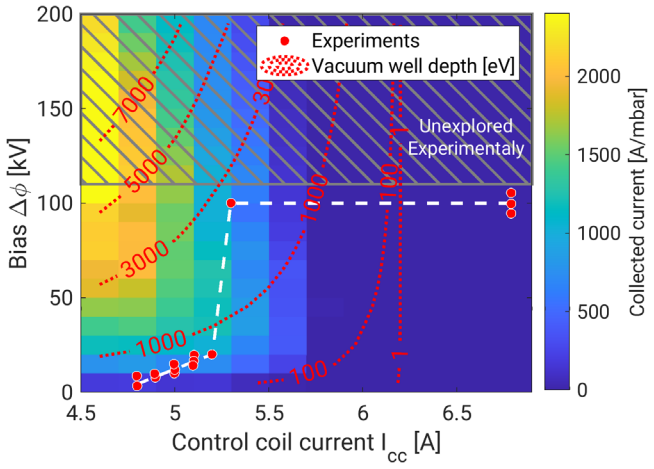

FIG. 6. Numerically measured total electronic current collected on the electrodes and stand-off voltage achieved in the experiments. The maximum voltage of 105 kV was limited by the PS capabilities and not the stand-off properties of the gun. The red dotted contour gives the maximum potential well depth in vacuum. The gray hatched rectangle shows the bias range unexplored experimentally due to PS limitations but explored numerically.

quadratic b-splines and an axially uniform grid of $\Delta z = 0.25$ mm, but radially non-uniform with $\Delta r = 0.05$ mm in the region of cloud trapping (between $59 < r < 65$ mm and $77 < r < 84$ mm), and $\Delta r = 0.25$ mm outside. The RNG is simulated as a uniform background of H_2 at room temperature and an enhanced neutral pressure $p_n = 1 \times 10^{-2}$ mbar to reduce simulation time, but low enough to ensure correct separation of the electron–neutral collisions timescales $\tau_{coll} \approx 8 \times 10^{-8}$ s and the electrons axial bounce timescale $\tau_b \approx L_{\parallel}/v_{th,\parallel} \approx 1 \times 10^{-8}$ s in the trap along the magnetic field lines. Here, $L_{\parallel}$ is the length of the cloud along the magnetic field line and $v_{th,\parallel}$ is the thermal parallel velocity. A reduced fluid model predicts that the steady state is reached due to the balance between the electron source caused by the RNG ionization, and the sink caused by radial drifts induced by azimuthal friction forces.[9] This model predicts a linear dependence between the collected current and the neutral gas density. For this reason, the measured current is then normalized by p_n. To confirm this proportionality, simulations have been run at different neutral gas pressure and the steady state current has been measured for the case with $\Delta\phi = 55$ kV and $I_{cc} = 4.8$A and is represented in Fig. 7. Each simulation was run on a 36 core node for ~12–36 h, depending on the bias and control coil parameters, until the system reaches a quasi-equilibrium. From the simulation results, the maximum electronic current collected on the electrodes was then calculated and is plotted as a rectangle on the color plot in Fig. 6. As mentioned earlier, these simulations neglect the ionic current but in steady state it is expected that this contribution will simply double the measured current and will not change the separation between regions, in the parameter space $(\Delta\phi, I_{cc})$, with and without problematic currents. When a strong current is observed, two electron clouds are present at the positions of local minima of potential well. As can be observed in Fig. 4, one cloud forms close to the cathode surface, while the other forms close to the anode. As seen in Fig. 5, each cloud changes the local potential well due to the clouds space charge, effectively reducing the potential well depth and its confinement properties. This can also allow electrons with high parallel velocity to exit the well along the magnetic field lines and lead to their collection on the anode surface.

As the total collected current was not measured during the experiments and the pressure in the vessel is uncertain, no direct comparisons of the current amplitude can be done between simulations and experiments. However, the simulation results show the same trend of high problematic currents for low I_{cc} and low or no problematic currents for high I_{cc}. Furthermore, the range of I_{cc} marking the limit between these two regions is in good agreement with the sharp decrease in the voltage stand-off at $I_{cc} = 5.3$A. The simulation results also show that, as in the experiments, a region exists where some potential well is present but no problematic current is measured between $I_{cc} = 5.3$ and $I_{cc} = 6.2$A. This is relevant for the development of future gyrotrons electron guns as it means that the current design criteria of avoiding any potential well in the gun region can be relaxed. To this end, FENNECS could be used as a useful design tool to predict the risk of problematic currents for a given gun geometry. We would

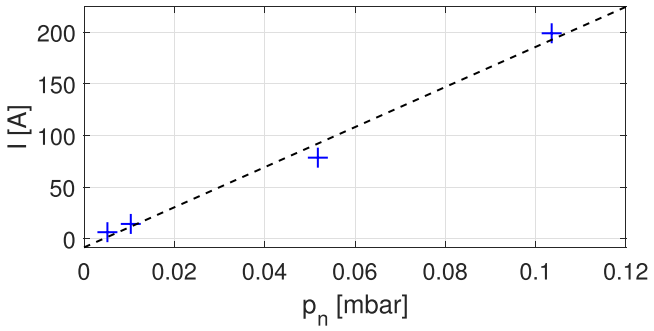

FIG. 7. Total electronic current collected on the electrodes in the steady state for various neutral gas pressures, for the case with $\Delta\phi = 55$ kV and $I_{cc} = 4.8$A (blue crosses). The black dashed line highlights the linear dependency.

like to remark that the formed annular electron clouds are susceptible to the diocotron instability that develops azimuthally and can, therefore, not be simulated in FENNECS.[18–20] However, the agreement between experiment and simulations is a strong sign that the diocotron instability might not play an important role for the amplitude of the collected current in this configuration, therefore supporting the use of axisymmetry for the simulations.

The extended scan in applied bias (gray hatched region in Fig. 6) gives further insight on the conditions of electron trapping. It shows that, for a given I_{cc}, increasing the bias voltage increases the collected current until a maximum is reached. If the bias is increased further, the collected current decreases again, which can lead to new regions where no problematic currents arise. This result, and the fact that for some potential wells no problematic current was observed, shows that the vacuum potential well depth and volume are not a sufficient measure to predict the amplitude of the current collected on the electrodes. This is visible by following the isolines of maximum potential well depth at 1 and 3 keV (Fig. 6), where a problematic current is observed for low I_{cc} but no problematic current is observed for high I_{cc}. The current hypothesis to explain this result is that larger bias $\Delta\phi$ increases the Larmor radius for the electrons, due to larger $\vec{E} \times \vec{B}$ velocity imposing a larger electron perpendicular velocity. This could lead to Larmor radii larger than the radial dimensions of the potential well and could limit the trapped electron cloud density by a reduction in the axial confinement.

In conclusion, we have shown that FENNECS can reproduce the same regions of problematic and non-problematic currents observed experimentally for the dummy-gun geometry. We have shown that a new region devoid of problematic currents could be accessed if the electric bias could be increased above the 105 kV experimental limit. However, this additional result still needs to be verified experimentally. A new flexible experiment called T-REX is being built at SPC.[21] This new experiment will study the electron cloud dynamics with more precise and dedicated diagnostics, allowing for different geometries and field topologies, and, thus, more direct comparisons between the simulations and experiments will be possible.

This work has been carried out within the framework of the EUROfusion Consortium, via the Euratom Research and Training Programme (Grant Agreement No. 101052200 — EUROfusion) and funded by the Swiss State Secretariat for Education, Research and Innovation (SERI). Views and opinions expressed are, however, those of the author(s) only and do not necessarily reflect those of the European Union, the European Commission, or SERI. Neither the European Union nor the European Commission nor SERI can be held responsible for them.

The calculations have been performed using the facilities of the Scientific IT and Application Support Center of EPFL.

This work was supported in part by the Swiss National Science Foundation under Grant No. 204631.

AUTHOR DECLARATIONS

Conflict of Interest

The authors have no conflicts to disclose.

Author Contributions

Guillaume Le Bars: Data curation (lead); Formal analysis (lead); Methodology (equal); Software (lead); Visualization (lead); Writing – original draft (lead). **Joaquim Loizu:** Conceptualization (equal); Formal analysis (equal); Funding acquisition (equal); Methodology (equal); Supervision (equal); Writing – review & editing (lead). **Jean-Philippe Hogge:** Conceptualization (equal); Funding acquisition (equal); Investigation (equal); Supervision (equal); Writing – review & editing (equal). **Stefano Alberti:** Conceptualization (equal); Funding acquisition (equal); Supervision (equal); Writing – review & editing (equal). **Francesco Romano:** Methodology (supporting); Supervision (supporting); Writing – review & editing (equal). **Jérémy Genoud:** Methodology (supporting); Supervision (supporting); Writing – review & editing (equal). **Ioannis Gr. Pagonakis:** Conceptualization (equal); Investigation (equal); Resources (equal); Writing – review & editing (equal).

DATA AVAILABILITY

The data that support the findings of this study are available from the corresponding author upon reasonable request.

REFERENCES

[1]T. Omori, M. A. Henderson, F. Albajar, S. Alberti, U. Baruah, T. S. Bigelow, B. Beckett, R. Bertizzolo, T. Bonicelli, A. Bruschi, J. B. Caughman, R. Chavan, S. Cirant, A. Collazos, D. Cox, C. Darbos, M. R. de Baar, G. Denisov, D. Farina, F. Gandini, T. Gassmann, T. P. Goodman, R. Heidinger, J. P. Hogge, S. Illy, O. Jean, J. Jin, K. Kajiwara, W. Kasparek, A. Kasugai, S. Kern, N. Kobayashi, H. Kumric, J. D. Landis, A. Moro, C. Nazare, Y. Oda, I. Pagonakis, B. Piosczyk, P. Platania, B. Plaum, E. Poli, L. Porte, D. Purohit, G. Ramponi, S. L. Rao, D. A. Rasmussen, D. M. S. Ronden, T. Rzesnicki, G. Saibene, K. Sakamoto, F. Sanchez, T. Scherer, M. A. Shapiro, C. Sozzi, P. Spaeh, D. Strauss, O. Sauter, K. Takahashi, R. J. Temkin, M. Thumm, M. Q. Tran, V. S. Udintsev, and H. Zohm, "Overview of the ITER EC H&CD system and its capabilities," Fusion Eng. Des. **86**, 951–954 (2011).

[2]C. Darbos, F. Albajar, T. Bonicelli, G. Carannante, M. Cavinato, F. Cismondi, G. Denisov, D. Farina, M. Gagliardi, F. Gandini, T. Gassmann, T. Goodman, G. Hanson, M. A. Henderson, K. Kajiwara, K. McElhaney, R. Nousiainen, Y. Oda, T. Omori, A. Oustinov, D. Parmar, V. L. Popov, D. Purohit, S. L. Rao, D. Rasmussen, V. Rathod, D. M. S. Ronden, G. Saibene, K. Sakamoto, F. Sartori, T. Scherer, N. P. Singh, D. Strauß, and K. Takahashi, "Status of the ITER electron cyclotron heating and current drive system," J. Infrared, Millimeter, Terahertz Waves **37**, 4–20 (2016).

[3]M. Q. Tran, P. Agostinetti, G. Aiello, K. Avramidis, B. Baiocchi, M. Barbisan, V. Bobkov, S. Briefi, A. Bruschi, R. Chavan, I. Chelis, C. Day, R. Delogu, B. Ell, F. Fanale, A. Fassina, U. Fantz, H. Faugel, L. Figini, D. Fiorucci, R. Friedl, T. Franke, G. Gantenbein, S. Garavaglia, G. Granucci, S. Hanke, J. P. Hogge, C. Hopf, A. Kostic, S. Illy, Z. Ioannidis, J. Jelonnek, J. Jin, G. Latsas, F. Louche, V. Maquet, R. Maggiora, A. Messiaen, D. Milanesio, A. Mimo, A. Moro, R. Ochoukov, J. Ongena, I. G. Pagonakis, D. Peponis, A. Pimazzoni, R. Ragona, N. Rispoli, T. Ruess, T. Rzesnicki, T. Scherer, P. Spaeh, G. Starnella, D. Strauss, M. Thumm, W. Tierens, I. Tigelis, C. Tsironis, M. Usoltceva, D. Van Eester, F. Veronese, P. Vincenzi, F. Wagner, C. Wu, F. Zeus, and W. Zhang, "Status and future development of heating and current drive for the EU DEMO," Fusion Eng. Des. **180**, 113159 (2022).

[4]C. Darbos, B. Beaumont, D. Boilson, M. Henderson, and C. Rotti, "Achievements and challenges for ITER heating & current drive systems," in 45th International Conference on Infrared, Millimeter, and Terahertz Waves (IRMMW-THz), 2020.

[5]K. R. Chu, "The electron cyclotron maser," Rev. Mod. Phys. **76**, 489–540 (2004).

[6]R. C. Davidson, *Physics of Nonneutral Plasmas* (World Scientific Publishing Co, 2001).

[7]M. Vogel, *Particle Confinement in Penning Traps,* Vol. 100 of Springer Series on Atomic, Optical, and Plasma Physics (Springer International Publishing, Cham, 2018).

[8]I. G. Pagonakis, B. Piosczyk, J. Zhang, S. Illy, T. Rzesnicki, J.-P. Hogge, K. Avramidis, G. Gantenbein, M. Thumm, and J. Jelonnek, "Electron trapping mechanisms in magnetron injection guns," Phys. Plasmas **23**, 023105 (2016).
[9]G. Le Bars, J.-P. Hogge, J. Loizu, S. Alberti, F. Romano, and A. Cerfon, "Self-consistent formation and steady-state characterization of trapped high-energy electron clouds in the presence of a neutral gas background," Phys. Plasmas **29**, 082105 (2022).
[10]B. Piosczyk, G. Dammertz, O. Dumbrajs, M. V. Kartikeyan, M. K. Thumm, and X. Yang, "165-GHz coaxial cavity gyrotron," IEEE Trans. Plasma Sci. **32**, 853–860 (2004).
[11]J. P. Hogge, S. Alberti, A. Arnold, D. Bariou, P. Benin, T. Bonicelli, A. Bruschi, R. Chavan, S. Cirant, O. Dumbrajs, D. Fasel, F. Gandini, E. Giguet, T. Goodman, R. Heidinger, M. Henderson, S. Illy, J. Jin, C. Lievin, R. Magne, P. Marmillod, P. L. Mondino, A. Perez, B. Piosczyk, L. Porte, T. Rzesnicki, M. Santinelli, M. Thumm, M. Q. Tran, and I. Yovchev, "Development of a 2-MW, CW coaxial gyrotron at 70 GHz and test facility for ITER," J. Phys.: Conf. Ser. **25**, 33–44 (2005).
[12]J.-P. Hogge, T. P. Goodman, S. Alberti, F. Albajar, K. A. Avramides, P. Benin, S. Bethuys, W. Bin, T. Bonicelli, A. Bruschi, S. Cirant, E. Droz, O. Dumbrajs, D. Fasel, F. Gandini, G. Gantenbein, S. Illy, S. Jawla, J. Jin, S. Kern, P. Lavanchy, C. LiÉvin, B. MarlÉtaz, P. Marmillod, A. Perez, B. Piosczyk, I. Pagonakis, L. Porte, T. Rzesnickl, U. Siravo, M. Thumm, and M. Q. Tran, "First experimental results from the European Union 2-MW coaxial cavity ITER gyrotron prototype," Fusion Sci. Technol. **55**, 204–212 (2009).
[13]I. G. Pagonakis, J. Hogge, T. Goodman, S. Alberti, B. Piosczyk, S. Illy, T. Rzesnicki, S. Kern, and C. Lievin, "Gun design criteria for the refurbishment of the first prototype of the EU 170GHz/2MW/CW coaxial cavity gyrotron for ITER," in 34th International Conference on Infrared, Millimeter, and Terahertz Waves, 2009.
[14]I. G. Pagonakis, J.-P. Hogge, S. Alberti, S. Illy, B. Piosczyk, S. Kern, C. Liévin, and M. Q. Tran, "Status of the EU 170 GHz/2 MW/CW coaxial cavity gyrotron for ITER: The dummy gun experiment," in 35th International Conference on Infrared, Millimeter, and Terahertz Waves, 2010.
[15]R. H. Fowler and L. Nordheim, "Electron emission in intense electric fields," Proc. R. Soc. London, Ser. A **119**, 173–181 (1997).
[16]K. Höllig, U. Reif, and J. Wipper, "Weighted extended B-spline approximation of Dirichlet problems," SIAM J. Numer. Anal. **39**, 442–462 (2001).
[17]J. P. Boris, and others. "Relativistic plasma simulation-optimization of a hybrid code," in *Proceedings of the Conference on the Numerical Simulation of Plasmas* (U.S. Naval Research Office, 1970), pp. 3–67.
[18]R. H. Levy, "Diocotron instability in a cylindrical geometry," Phys. Fluids **8**(7), 1288 (1965).
[19]G. N. Kervalishvili, J. I. Javakhishvili, and N. A. Kervalishvili, "Diocotron instability in an annular sheath of a gas-discharge nonneutral electron plasma," Phys. Lett. A **296**, 289–294 (2002).
[20]G. Rosenthal, G. Dimonte, and A. Y. Wong, "Stabilization of the diocotron instability in an annular plasma," Phys. Fluids **30**, 3257–3261 (1987).
[21]F. Romano, S. Alberti, J.-P. Hogge, J. Genoud, G. L. Bars, and J. Loizu, "The TRapped Electrons eXperiment (T-REX)," in 13th International Workshop on Non-Neutral Plasmas, Milano, 2022.